Research Square

Preprints are preliminary reports that have not undergone peer review.
They should not be considered conclusive, used to inform clinical practice,
or referenced by the media as validated information.

Entangled Photons, Gravitational Records, and Correlated Kerr Horizon-Area Changes

Pablo Garcia Tello

pablo.garcia.tello@cern.ch

European Organization for Nuclear Research

Research Article

Keywords:

Posted Date: November 19th, 2026

DOI: https://doi.org/10.21203/rs.3.rs-11610412/v1

License: This work is licensed under a Creative Commons Attribution 4.0 International License.
Read Full License

Additional Declarations: No competing interests reported.

Entangled Photons, Gravitational Records, and Correlated Kerr Horizon-Area Changes

Pablo Garcia Tello,
CERN CH-1211 Geneva 23, Switzerland,
pablo.garcia.tello@cern.ch

Abstract

We examine how local gravitational interactions redistribute information initially encoded in the paths of an entangled photon pair. A controlled-recoil model relates the surviving two-photon coherence to the overlap of the alternative mass records. Replacing the masses by rotating black holes gives a distinct area-response problem: the Kerr first law predicts unequal horizon-area increments for equal-energy deposits with opposite axial angular momenta. In a symmetric two-hole geometry the joint alternatives exchange these increments, producing anticorrelated area responses with a common total. An effective capture map connects the two alternatives to conditional absorption amplitudes and external records. For identical local responses, unequal prograde and retrograde capture efficiencies do not unbalance the post-selected joint branches; the surviving two-hole coherence depends on the distinguishability of the remaining records. We derive the area-outcome covariance and an operationally motivated phase-sensitive witness, showing why area correlations alone cannot distinguish a coherent state from a diagonal mixture. The calculation combines a classical Kerr benchmark with an explicitly conditional quantum model; the absorption amplitudes and physical access to the proposed phase observable remain dynamical questions.

1 Introduction

A local interaction can change a particle's momentum even when its state is entangled with a distant system. The apparent tension dissolves once the states of the interacting systems are included, but the physical location of the resulting information depends on which degrees of freedom can

carry records and which measurements are permitted. When the interacting objects gravitate, this bookkeeping cannot automatically identify an object and its gravitational field as independent subsystems. Gravitationally dressed observables and the constraints associated with them make localization and factorization nontrivial, even in perturbation theory [1].

Black holes make the question more concrete and more difficult. Danielson, Satishchandran and Wald studied a spatially superposed exterior body whose long-range field couples to a black-hole horizon and creates a which-path record [2]. Their body remains outside the hole; their mechanism is not a calculation of the absorption of an incoming photon. Foo, Mann and Zych study quantum superpositions of black-hole geometries and, in a separate model, the signatures of a superposed black-hole mass spectrum [3, 4]. Their discussion of a superposition-basis or ancilla measurement supplies a useful comparison, not an established readout for a pair of rotating holes. Liu and collaborators examine radiation-mediated entanglement between black holes in different, holographic models [5]. Brádler and Adami study horizon interactions as quantum information channels, including limiting cases of perfect absorption and reflection [6]. Gralla and Wei calculate electromagnetic and scalar analogues of horizon-induced decoherence for rotating black holes [7]. These results address different physical inputs from the paired, capture-conditioned Kerr comparison developed here.

We ask what can be said about records and coherence when two initially path-entangled photons interact locally with distant massive systems and, in a second version, are absorbed by rotating black holes. Our contribution is the linked analysis of these encounters in a common geometry. The Kerr first law determines a pair of exchanged area responses; an explicit local capture map then relates their conditional branch weights to the absorption amplitudes and the overlap of remaining records. This construction makes a concrete distinction between area-outcome correlations and the phase-sensitive correlations required to establish entanglement. In particular, for identical local capture responses the two joint alternatives have equal conditional weight even when the aligned and opposed capture probabilities differ. The resulting benchmark and witness do not require an assumed area spectrum. These results combine established components in a specific two-hole setting; their distinctiveness lies in the comparison and derived conditional relations rather than in a new law of black-hole mechanics.

Our treatment combines classical Kerr mechanics with quantum-information models of local in-

teraction and conditional capture. The numerical examples evaluate analytic formulas for specified inputs. We use SI units except where geometrized variables are explicitly introduced.

2 Geometry and assumptions

Place a source near the origin of an approximately inertial common coordinate system, and locate two well-separated systems, A and B, near $x = +D$ and $x = -D$. Photon A propagates approximately in the $+x$ direction and photon B in the $-x$ direction. The label U (D) identifies an incoming wavepacket passing on the $y > 0$ ($y < 0$) side of its own local centre. The paths are therefore defined by common global signs, not by the direction of a later deflection. The incoming ideal state is

$$|\Psi_\gamma\rangle = \frac{1}{\sqrt{2}}\big(|U\rangle_A|U\rangle_B + |D\rangle_A|D\rangle_B\big). \tag{1}$$

The wavepackets U, D on each side are taken to be orthogonal. Their equal amplitudes and phase coherence are preparation assumptions. Any distinguishing record left by the source or its support is initially negligible, or is retained explicitly in a larger state. Figure 1 depicts the sign conventions, not actual trajectories.

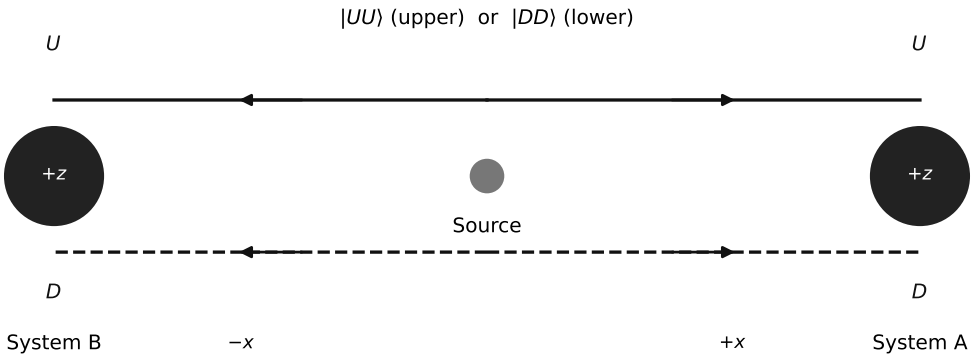


Figure 1: Schematic geometry for both versions of the thought experiment. System A lies to the right and B to the left of the source. Solid upper and dashed lower lines label the U and D incoming sides in a common coordinate system; arrows indicate opposite directions of photon propagation. The ideal state contains the joint alternatives UU and DD, not four independent classical rays. In the Kerr version both spin axes point along global $+z$, normal to the plane. The lines are diagrammatic and are not computed geodesics; their apparent discontinuity at the source represents preparation of spatially separated wavepackets.

One may arrange the principal local encounters to be spacelike separated: if their spatial separation in the chosen frame is ℓ and their time difference is Δt, this requires $\ell > c|\Delta t|$. The correlated preparation is in their common past. Long-range fields exist before closest approach, so this condition refers to chosen local regions or events, not to the entirety of the field histories. Neither local outcome is controlled by the remote measurement choice. Any later comparison of data requires causal communication.

For the absorption example the systems are identical, nonextremal Kerr black holes whose spins point along global $+z$. The holes are assumed sufficiently separated that each interaction is approximated by a local Kerr problem. We do not construct an exact two-hole stationary solution or specify the supports and external fields required to prepare such a configuration. Write $L > 0$ for the magnitude of the approximate orbital angular momentum about a local hole. Since $L_z = xp_y - yp_x$ and the directions of propagation are opposite,

$$UU:\ (L_{z,A}, L_{z,B}) \simeq (-L, +L), \qquad DD:\ (L_{z,A}, L_{z,B}) \simeq (+L, -L). \tag{2}$$

The approximation refers to wavepackets centred on the indicated impact parameters, not exact orbital-angular-momentum eigenstates. Photon spin and the spread in L_z are neglected at leading order. One hole is aligned and the other opposed in each joint alternative.

The geometric and sharp-charge descriptions require different idealizations. A packet localized on one side of a hole is generally a superposition of axial angular-momentum modes. For a narrow paraxial packet on a plane through the local centre, $L_z \simeq -yp_x$; if the transverse position width is σ_y, its orbital spread is of order $|p_x|\sigma_y$. Thus $\sigma_y \ll |b|$ gives a spread small relative to the central magnitude $|L_z| \simeq |bp_x|$, but not a state of exactly sharp L_z. The local charge eigenstates used later in the witness discussion are an effective mode idealization. A wavepacket calculation would retain the distribution over allowed total axial-angular-momentum eigenvalues and photon helicities. The assumption that the two joint branches have exactly matching total charges must be imposed on those mode amplitudes; it is not a consequence of assigning the same central impact parameter.

3 Deflection and recoil records

First suppose that the systems are ordinary spherical masses and that each photon passes outside its object. In the weak-field, small-angle limit, for mass M, impact parameter b and photon energy E, the leading deflection and the magnitude of the transverse momentum transfer are

$$\vartheta \simeq \frac{4GM}{bc^2}, \qquad k \simeq \frac{E}{c}\vartheta. \tag{3}$$

The first expression is the leading Einstein bending angle [8]. The photon bends toward the local centre, so an upper path receives a downward photon deflection and the ideal mass recoil points upward; a lower path gives the reverse. In a complete scattering problem the field, radiation, the supports and other apparatus can also participate in the momentum balance. Assigning the full transverse recoil $\pm k$ to a centre-of-mass state is an isolated controlled-kick approximation.

Let $|u\rangle$ and $|d\rangle$ denote orthogonal outgoing photon modes associated with the incoming U, D alternatives. Assume initially pure, independent mass states and local unitary interactions with normalized final recoil states $|M_i^+\rangle$ and $|M_i^-\rangle$ for $i = A, B$. The signs label the *mass* kicks. Ignoring additional records, the joint final state has the form

$$|\Psi\rangle = \frac{1}{\sqrt{2}}\left(|uu\rangle|M_A^+ M_B^+\rangle + e^{i\phi}|dd\rangle|M_A^- M_B^-\rangle\right), \tag{4}$$

where ϕ includes the initial relative phase and any branch-dependent dynamical phases. This expression assumes that within each branch the photon and local mass states factorize. General scattering can instead produce entanglement within each branch and a more complicated reduced state.

Define $\gamma_i = \langle M_i^-|M_i^+\rangle$. Tracing out the masses gives

$$\begin{aligned}\rho_{\gamma\gamma} = {} & \tfrac{1}{2}|uu\rangle\langle uu| + \tfrac{1}{2}|dd\rangle\langle dd| \\ & + \tfrac{1}{2}e^{-i\phi}\gamma_A\gamma_B|uu\rangle\langle dd| + \tfrac{1}{2}e^{i\phi}\gamma_A^*\gamma_B^*|dd\rangle\langle uu|.\end{aligned} \tag{5}$$

Its off-diagonal magnitude is $|\gamma_A\gamma_B|/2$. For this two-branch density matrix the concurrence is

$$C_{\gamma\gamma} = |\gamma_A\gamma_B|. \tag{6}$$

To see the result without invoking a general formula, the state is supported on $|uu\rangle, |dd\rangle$ and its only coherence between those alternatives has magnitude $|\gamma_A\gamma_B|/2$; the two-qubit concurrence is twice that magnitude. If the two photons are locally recombined and their coincidence correlations are measured as a function of a joint phase, the corresponding ideal visibility is $V_{AB} = |\gamma_A\gamma_B|$. An individual photon's reduced state is balanced and has no single-photon path fringe in this model.

For equal-prior pure joint mass records, their optimal trace-distance distinguishability is $D_M = \sqrt{1 - |\gamma_A\gamma_B|^2}$, giving

$$D_M^2 + V_{AB}^2 = 1. \tag{7}$$

This is a special pure-record instance of the established visibility–which-way relation [9]. The optimal measurement may act jointly on both mass records. Equation (7) is not a statement that either observer can learn the remote result without comparing data. If a record becomes perfectly distinguishable, $C_{\gamma\gamma}$ vanishes but the photon path outcomes remain correlated. Conversely, a nonzero local momentum change does not itself imply an orthogonal record.

The complete system also matters. Under the independent local unitary model, the entanglement across the partition (photon A + mass A) | (photon B + mass B) is unchanged from the initially pure state. Entanglement between the *photons alone* can decrease because it is redistributed among larger systems. This statement assumes local unitary dynamics and initially uncorrelated local ancillas; it does not follow from classical momentum conservation alone.

For a concrete record-overlap estimate, take a one-dimensional pure Gaussian mass position distribution of standard deviation σ_x and instantaneous momentum kicks $\pm k$. The overlap is the characteristic function of the position distribution evaluated at $2k/\hbar$:

$$|\gamma| = \left| \int \mathrm{d}x \, |\psi(x)|^2 e^{2ikx/\hbar} \right| = \exp\left[-2 \left(\frac{k\sigma_x}{\hbar} \right)^2 \right]. \tag{8}$$

The mean position can add a phase but not change the magnitude. For two identical independently prepared masses, $C_{\gamma\gamma} = |\gamma|^2$. This example is not an assertion that a macroscopic astronomical

object can be prepared in the postulated pure state.

If a mass starts mixed, its two reduced recoil states may be hard to distinguish even though a purifying environment or conditional phases suppress photon coherence. Equality in Eq. (7) then need not hold for mass-only measurements. Further source, support, radiation or field records alter Eq. (5); multiplying their overlaps is justified only when the relevant conditional record state factorizes. The field of a source cannot simply be counted as an independent record in addition to that source. Danielson *et al.* discuss the subtle distinction between long-range and radiative field contributions, particularly at finite times [2]; the perturbative dressing problem gives a related warning [1].

3.1 An illustrative recoil scale

Take $M = 2.0 \times 10^{30}\,\mathrm{kg}$, radius $5.0 \times 10^{8}\,\mathrm{m}$, impact parameter $b = 1.0 \times 10^{9}\,\mathrm{m}$ and $E = 1.0\,\mathrm{keV}$. These are selected model inputs. The photon passes outside the object, and $GM/(bc^2) \simeq 1.5\times10^{-6}$. Equation (3) gives $\vartheta \simeq 5.9\times10^{-6}\,\mathrm{rad}$ and $k \simeq 3.2\times10^{-30}\,\mathrm{kg\,m\,s^{-1}}$. With independent pure Gaussian states of width $\sigma_x = 10^{-5}\,\mathrm{m}$, $k\sigma_x/\hbar \simeq 0.30$, giving $|\gamma| \simeq 0.83$ and $C_{\gamma\gamma} \simeq 0.70$. Constants are from the 2022 CODATA compilation [10]. These figures illustrate sensitivity to a dimensionless model parameter; they do not estimate experimental preparation, isolation or measurement errors.

4 Rotating black holes: a classical absorption benchmark

We now replace the masses with Kerr black holes. Each is initially specified by mass M, angular momentum J and dimensionless spin $a_* = cJ/(GM^2)$, with $0 < a_* < 1$. The geometric length $r_g = GM/c^2$ and the dimensionless quantity $s = \sqrt{1 - a_*^2}$ give the outer-horizon radius $r_+ = r_g(1 + s)$, the area $A = 8\pi r_g^2(1 + s)$, the horizon angular velocity Ω_H and the physical surface gravity κ as [11]

$$\Omega_H = \frac{c}{r_g}\frac{a_*}{2(1+s)}, \qquad \kappa = \frac{c^2}{r_g}\frac{s}{2(1+s)}. \tag{9}$$

Here κ has units of acceleration and Ω_H of inverse time. These formulas concern stationary, uncharged Kerr solutions.

For changes between nearby stationary states, the first law of black-hole mechanics is [12]

$$\Delta A \simeq \frac{8\pi G}{\kappa c^2}(E - \Omega_H L_z). \tag{10}$$

In this expression E and L_z are the energy and axial angular momentum actually deposited in the hole. In an isolated stationary comparison they are the changes in the black-hole energy Mc^2 and angular momentum J. Setting them equal to the incident photon's values is an idealization that neglects escaping radiation, recoil and energy or angular momentum carried by supports. The initial κ and Ω_H are used because Eq. (10) is linearized; it is not an instantaneous local area measurement.

For equal deposited energy E and angular momenta $L_z = \pm L$, define

$$A_0 = \frac{8\pi G E}{\kappa c^2}, \qquad \alpha = \frac{\Omega_H L}{E}. \tag{11}$$

The aligned and opposed area responses are then

$$\Delta A_+ = A_0(1 - \alpha), \qquad \Delta A_- = A_0(1 + \alpha). \tag{12}$$

The $+$ or $-$ subscript denotes the sign of angular momentum *relative to the spin*, not the sign of the area change. Within this classical benchmark, the opposed deposit produces the greater area increase. If $0 < \alpha < 1$, both are positive. This condition is satisfied by the example below; it is not asserted for arbitrary incident Kerr modes.

Using Eq. (2), and assuming equal deposited energy and equal $|L_z|$ in both encounters, gives

$$UU: \ (\Delta A_A, \Delta A_B) = (\Delta A_-, \Delta A_+), \qquad DD: \ (\Delta A_A, \Delta A_B) = (\Delta A_+, \Delta A_-). \tag{13}$$

Consequently $\Delta A_A + \Delta A_B = 2A_0$ in either alternative at this order. The correlated alternative is the allocation of the larger increase, not a difference in the leading total increase. In the comparison of *independent* identical Kerr holes, the equality of the sum is actually exact for finite deposits that lead to the exchanged final parameters: each branch contains the same two final Kerr configurations in the opposite order. This permutation argument is separate from the first-order value $2A_0$; it

does not assert an exact two-hole solution.

The difference between the two local responses provides a useful spin-sensitive form of the first law. Combining Eqs. (9)–(12) gives

$$\Delta A_- - \Delta A_+ = \frac{16\pi G a_* L}{c^3\sqrt{1-a_*^2}} = 16\pi\ell_P^2 \frac{a_*}{\sqrt{1-a_*^2}}\frac{L}{\hbar}, \tag{14}$$

where $\ell_P^2 = \hbar G/c^3$. The expression is first order in the deposits and applies to a nonextremal hole. The increasing coefficient near extremality does not license taking the extremal limit at fixed perturbation: the perturbation must remain small compared with the distance to extremality for the linear expansion to apply. In the nonrotating limit the first-order area splitting vanishes. For an initially Schwarzschild hole, the exact stationary Kerr area is also even in the final angular momentum, so equal-energy deposits with $+L$ and $-L$ produce equal areas in this ideal comparison, although their final angular momenta remain distinct. Initial rotation is therefore essential for the particular area-label distinction considered here. The common-sum result depends on identical initial holes and symmetric actual deposits; escaping radiation or unequal deposits can break it.

4.1 A capture check, not an absorption calculation

Choose $a_* = 1/2$ and signed impact parameters $b = \pm r_g$. The geometrical-optics estimate $L \simeq E|b|/c$ gives

$$\alpha \simeq \frac{a_*}{2(1+\sqrt{1-a_*^2})} = 0.133975\ldots, \tag{15}$$

so the response factors are $\Delta A_+/A_0 \simeq 0.8660$ and $\Delta A_-/A_0 \simeq 1.1340$. The positive horizon-energy factors $1 \mp \alpha$ are consistent with the classical capture condition in this example.

It is necessary to check that both signed rays can reach the horizon. For an equatorial null geodesic, the Kerr radial potential contains the cubic written in Appendix A [13]. For the selected a_* and $b/r_g = \pm 1$, this cubic is positive and increasing outside the outer horizon for both signs. An ingoing test ray therefore has no exterior radial turning point. This does not calculate a finite wavepacket's absorption probability, photon helicity effects or the outgoing state. Wave absorption by a rotating hole is mode-dependent, and superradiance occurs in other parameter regimes [8]. The positive classical horizon-energy factor here should not be mistaken for a general quantum

absorption amplitude.

4.2 Area scales

Let $M = 2.0 \times 10^{30}\,\mathrm{kg}$ and take the *deposited* energy to be $E = 1.0\,\mathrm{keV}$, with $a_* = 1/2$ and $L \simeq E r_g/c$. Then $r_g \simeq 1.49 \times 10^3\,\mathrm{m}$, the incident photon wavelength is approximately $1.24 \times 10^{-9}\,\mathrm{m}$, and $E/(Mc^2) \simeq 8.9 \times 10^{-64}$. The geometrical-optics wavelength is much shorter than r_g, and the deposit is a very small perturbation of the hole's energy. The orbital scale is $L/\hbar \simeq 7.5 \times 10^{12}$, so the photon's spin is negligible in the leading orbital sign and magnitude estimate; neither statement resolves the wavepacket's angular-momentum spread.

Equations (9)–(12) give

$$\Delta A_+ \simeq 1.84 \times 10^{-55}\,\mathrm{m}^2, \qquad \Delta A_- \simeq 2.41 \times 10^{-55}\,\mathrm{m}^2. \tag{16}$$

The difference is about $5.7 \times 10^{-56}\,\mathrm{m}^2$, or 2.2×10^{14} times $\ell_P^2 = \hbar G/c^3$. These are calculated benchmark values, not observations or predicted measurement precision. Their scale in Planck units does not establish that the quantum states are distinguishable. The answer depends on the initial state, dynamics and actual observable. For comparison, a linearized-gravity calculation for a Schwarzschild hole in a Hartle–Hawking state gives an area standard deviation $\sigma_A \simeq \sqrt{8\pi}\, r_H \ell_P$ for a particular area observable [14]. At the mass chosen here, its scale is $\sim 2.4 \times 10^{-31}\,\mathrm{m}^2$, much larger than the calculated splitting. The state, observable and geometry differ from our Kerr model, so this comparison is not a universal bound on distinguishability; it illustrates why the relevant quantum state and its area fluctuations must be specified.

5 A conditional quantum description of two holes

The first law is a relation between classical stationary solutions. It neither constructs a quantum area operator nor establishes orthogonal black-hole states corresponding to the two responses. To formulate, rather than presume, a coherence question, introduce two normalized effective states for each hole, $|B_+\rangle$ and $|B_-\rangle$, associated respectively with the aligned and opposed deposits. Assume for the following toy model that these two states are orthogonal locally and that an approximate

tensor-product separation of the two holes and all other degrees of freedom is meaningful. The association of the labels with exact area eigenstates is not required and is not demonstrated.

The following local isometry makes the origin of the branch amplitudes explicit. Let $t_{i\pm}$ be the complex amplitudes for a photon with the indicated sign of L_z to be captured at hole $i = A, B$, and let $|r_{i\pm}\rangle$ be normalized conditional records outside the selected black-hole state. In a simplified mode-diagonal instrument, the successful part of the local interaction is

$$|\pm\rangle_{\gamma i}|B_0\rangle_i|r_{i0}\rangle \longmapsto t_{i\pm}|\mathrm{vac}\rangle_{\gamma i}|B_\pm\rangle_i|r_{i\pm}\rangle + |\mathrm{fail}_{i\pm}\rangle. \tag{17}$$

The failure component is orthogonal to the selected local capture outcome, and the full map is assumed to extend to an isometry. Thus $0 \le |t_{i\pm}|^2 \le 1$ and the norm squared of the failure component is $1 - |t_{i\pm}|^2$. The labels $\pm$ here denote the *local angular-momentum sign*, not the incoming-side labels U, D. This is a phenomenological quantum instrument: it specifies how to track coherences once amplitudes and states are given, rather than computing a Kerr absorption channel. The environment factorization in Eq. (17) is also an additional assumption; a gravitationally dressed description need not have this simple structure [1].

For the input of Eq. (1), define $q_1 = t_{A-}t_{B+}$ and $q_2 = t_{A+}t_{B-}$. If the local initial systems and records are independent and the selected black-hole labels are orthogonal, the probability of joint successful capture is

$$P_{\mathrm{cap}} = \frac{|q_1|^2 + |q_2|^2}{2}. \tag{18}$$

For $P_{\mathrm{cap}} > 0$, $c_1 = q_1/\sqrt{|q_1|^2 + |q_2|^2}$ and $c_2 = q_2/\sqrt{|q_1|^2 + |q_2|^2}$. In particular, if the capture probabilities are matched between the two local systems, $|t_{A\pm}|^2 = |t_{B\pm}|^2 = \eta_\pm$, then $|q_1|^2 = |q_2|^2 = \eta_-\eta_+$ and

$$P_{\mathrm{cap}} = \eta_-\eta_+, \qquad |c_1|^2 = |c_2|^2 = \tfrac{1}{2}, \tag{19}$$

even when $\eta_+ \neq \eta_-$. The complex phases of q_1 and q_2 need not be equal; their difference contributes to the conditional relative phase. Equal branch weights therefore follow from this matched-probability model, not from the initial Bell amplitudes alone. Whether the required equality holds for actual incoming modes, polarizations and local environments is a dynamical question. Independent local record states give $|R_1\rangle = |r_{A-}r_{B+}\rangle$ and $|R_2\rangle = |r_{A+}r_{B-}\rangle$; more general shared or

correlated records are accommodated below without factorizing their overlap. Joint postselection is identified by later comparison of local outcomes and does not enable signalling.

Conditioning on successful absorption at both holes, consider the normalized pure state

$$|\Psi_f\rangle = c_1|B_-\rangle_A|B_+\rangle_B|R_1\rangle + c_2|B_+\rangle_A|B_-\rangle_B|R_2\rangle, \quad |c_1|^2 + |c_2|^2 = 1. \tag{20}$$

The normalized $|R_1\rangle$ and $|R_2\rangle$ represent source, apparatus, field and radiation degrees of freedom in the chosen factorization. Equation (18) provides one explicit realization; Eq. (20) also allows nonfactorized records and general conditional coefficients. The coefficients and $\langle R_2|R_1\rangle$ are not determined by the classical Kerr calculation. Local filtering can change conditional entanglement without creating entanglement on average by local operations alone.

With $|0\rangle = |B_-\rangle$ and $|1\rangle = |B_+\rangle$, trace over R and define $p = |c_1|^2$ and $z = c_1c_2^*\langle R_2|R_1\rangle$. Then

$$\rho_{AB} = p|01\rangle\langle 01| + (1-p)|10\rangle\langle 10| + z|01\rangle\langle 10| + z^*|10\rangle\langle 01|. \tag{21}$$

Positivity imposes $|z| \leq \sqrt{p(1-p)}$. The two-qubit concurrence for this exact two-alternative state is

$$C_{AB} = 2|z| = 2|c_1c_2|\,|\langle R_2|R_1\rangle|. \tag{22}$$

For equal amplitudes and pure normalized external records, their optimal equal-prior distinguishability is $D_R = \sqrt{1 - |\langle R_2|R_1\rangle|^2}$. The conditional two-hole concurrence then satisfies

$$C_{AB}^2 + D_R^2 = 1. \tag{23}$$

Thus the same record–coherence relation encountered in the recoil model reappears after ideal absorption, with the external records rather than the masses traced out. For unequal amplitudes, $C_{AB} = 2\sqrt{p(1-p)}\,|\langle R_2|R_1\rangle|$. For mixed outside records or nonorthogonal local black-hole states, Eq. (22) requires modification. Purification can be included in R as a mathematical description, provided the resulting subsystem split is physically justified.

5.1 Correlated areas versus a phase-sensitive observable

A measurement that only distinguishes the two area-response labels yields probabilities p and $1-p$ for 01 and 10. The phenomenological record mixture

$$\rho_{\mathrm{mix}} = p|01\rangle\langle 01| + (1-p)|10\rangle\langle 10| \tag{24}$$

has exactly the same area-outcome probabilities as Eq. (21). It may be represented by correlated local path records followed by the corresponding classical Kerr responses. Let $\mathcal{A}_A, \mathcal{A}_B$ denote the respective response labels in this ideal two-outcome comparison. Equation (13) yields

$$\begin{aligned} \mathrm{Cov}(\mathcal{A}_A, \mathcal{A}_B) &= -4p(1-p)(A_0\alpha)^2, \\ \mathrm{Var}(\mathcal{A}_A + \mathcal{A}_B) &= 0. \end{aligned} \tag{25}$$

For $0 < p < 1$ and $\alpha \neq 0$, the ideal area-response outcomes are perfectly anticorrelated. The same covariance follows from the coherent state and the mixture because it depends only on p, not on z. In an actual experiment, the measured area or charge distributions would include initial-state uncertainty, finite wavepacket widths and other noise; Eq. (25) concerns the idealized two-response labels. The measure-and-record comparison shows precisely which joint statistics are insensitive to the phase without requiring a complete hybrid theory of backreacting classical gravity.

The operator

$$W_\theta = e^{i\theta}|01\rangle\langle 10| + e^{-i\theta}|10\rangle\langle 01| \tag{26}$$

has expectation $\langle W_\theta\rangle = 2\,\mathrm{Re}(e^{-i\theta}z)$. A calibrated phase scan in the toy model is therefore sensitive to both quadratures of the coherence, whereas the particular diagonal mixture gives zero for every θ. For $\theta = 0$,

$$W_0 = \tfrac{1}{2}(X_A X_B + Y_A Y_B), \tag{27}$$

where X_i, Y_i are Pauli operators in the assumed local $\{|0\rangle, |1\rangle\}$ spaces. For any separable state in the full two-qubit space,

$$|\langle W_0\rangle| \leq \tfrac{1}{2}. \tag{28}$$

Indeed, for a product state the expectation is half the scalar product of the transverse components of the two local Bloch vectors; each has length at most one, and convexity extends the bound to mixtures. A value exceeding $1/2$ is therefore an entanglement witness if the qubit description and measurement calibration apply. In the exact subspace spanned by $01, 10$, any nonzero z implies entanglement; outside it, nonzero $\langle W_0 \rangle$ alone does not exclude all separable states. A practical test would also need to account for capture-conditioned sampling, other outcomes and imperfect measurements.

This operator is an algebraic diagnostic, not an identified measurement on real holes. In the symmetric benchmark the two joint alternatives have the same total deposited energy and axial angular momentum. If both joint alternatives lie in the same sharp total-charge sectors, W_θ commutes with those total charges in the reduced model. This conclusion requires matching the actual angular-momentum mode labels, not merely their geometric-optics mean values. Local X or Y measurements nevertheless mix states differing by $2L$ in their local deposited angular momenta. Any physical operation would need angular-momentum references, a relative phase standard, and an account of their recoil and field records. The global charge observation does not construct such an operation.

A further obstacle is the classical area theorem under its assumptions [15]. A literal swap between settled classical Kerr labels at fixed energy would lower one hole's area. A quantum measurement need not be a literal classical swap, but an implementation would have to account for the theorem's domain, auxiliary systems and possible quantum effects rather than simply asserting a swap. More fundamentally, arbitrary interior degrees of freedom are not available to an exterior observer. A viable protocol must specify exterior or relational observables, or a process that transfers the coherence to accessible radiation. The superposition-basis and ancilla proposal in the distinct mass-superposition model of Foo *et al.* is informative but does not establish this operation for the two Kerr holes [4]. The settled event horizon and its area are global spacetime properties, so the spacelike arrangement of the absorption events does not itself prove that final-area measurements are local spacelike events.

6 Discussion

6.1 What the records do and do not show

The two examples answer different versions of the information question. In the controlled-recoil model, Eq. (5) gives a complete reduced photon state under explicit assumptions, so the effect of the mass-record overlap can be calculated. In the Kerr example, Eqs. (12) and (13) establish only a classical relation between nearby stationary configurations. The distinction is consequential: the calculation of a nonzero area difference does not say whether the two associated quantum states are orthogonal, whether coherence between them survives, or whether the coherence can be observed.

One can replace the holes by ordinary local quantum memories that absorb photons and retain their path labels. In an ideal unitary absorption model the memories can inherit entanglement initially carried by the photons without an interaction between the memories. The analogy shows why final-state entanglement, even if established, would not by itself show that gravity *created* entanglement or transmitted quantum information between A and B. The input here is already entangled. The analogy treats photons and memories quantum mechanically in a prescribed background; it is not a complete theory of gravity coupled to quantum matter.

A classical-channel model of gravity due to Kafri, Taylor and Milburn cannot create entanglement between initially unentangled resonators under that model's measurement-and-feedback assumptions [16]. That result addresses a different initial state and interaction from ours. Our diagonal-record comparison is likewise model-specific; it does not establish a no-go theorem for every possible classical-field or hybrid theory. A stronger discrimination between gravitational theories would require a defined competing dynamical model and measurements beyond the area-basis frequencies.

A possible conceptual connection is the ER=EPR proposal, according to which certain entangled black-hole states admit a description involving an Einstein–Rosen bridge, with a more general quantum connection conjectured for other entangled systems [17]. If the conditional absorption process considered here produces an entangled two-hole state, it is natural to ask whether that state admits a geometric description of this kind. Our model does not answer that question: it specifies neither the complete black-hole microstate nor an interior geometry, and entanglement alone does not generally establish a semiclassical wormhole [18]. In particular, the classical horizon-

area changes calculated here should not be identified with the area of a bridge throat. The proposed connection is therefore interpretive and does not alter the local account of the interactions or imply communication between the holes.

Path information can in principle be reflected in mass recoil, black-hole angular momentum, the exterior geometry, or radiation, depending on the model and the accessible observables. These categories need not be independent copies. A gravitationally dressed excitation necessarily involves its field, and perturbative localization results have restricted assumptions [1]. Danielson *et al.* show how a black-hole horizon can acquire which-path information in a different arrangement involving an exterior superposed body [2]. Their calculation motivates including field and horizon records, but supplies neither the $|R_i\rangle$ overlap nor a decoherence rate for our photon-absorption process.

In the conditional model the phase information retained by the selected two-hole state is encoded in z. If $\langle R_2|R_1\rangle = 0$, that phase is absent from the two-hole reduced density matrix. Under the assumed globally pure unitary description the branch phase may still be represented in the joint state including R, but no recovery operation is given. This two-branch example should not be used to claim that an arbitrary unknown quantum state can be hidden exclusively in correlations. The no-hiding theorem concerns unitary encodings of arbitrary inputs whose information is completely absent from one subsystem [19]; its conditions and conclusion are distinct from the present restricted construction.

6.2 Area, entropy and spectra

Black-hole entropy associated with horizon area, a hypothesized microscopic degeneracy at a given area, and entanglement between our two effective alternatives are distinct concepts. Equation (22) describes only the last, under a specified two-qubit model. It cannot be read as a change of thermodynamic entropy, and the classical area variation cannot by itself quantify the recoverable photon information.

The correspondence-principle proposal of Hod assigns a specific spacing to a Schwarzschild area spectrum [20]; Maggiore's alternative interpretation of quasinormal-mode frequencies leads to a different spacing [21]. Models of Kerr area quantization have also been developed using additional spectral assumptions [22]. We do not assume a particular spacing in the present calculation. Bohr's correspondence principle in that discussion is also different from the which-way–visibility

complementarity used in Sec. 3. The large area difference in Planck units in Eq. (16) is therefore not an eigenstate counting or distinguishability argument.

6.3 Principal limitations and next theoretical steps

The analysis separates a benchmark from an open dynamical problem. The weak-field recoil calculation assumes a clean controlled kick and pure, factorized Gaussian records; an interacting gravitational field, radiation, a mixed mass and source recoil can all invalidate the simple overlap product. The Kerr calculation assumes small deposits between stationary states, identical well-separated holes, a geometric-optics centre for each packet and neglect of radiative loss. Event-horizon area is a global quantity; the simplified treatment does not solve the full dynamical spacetime. The $\pm r_g$ capture check uses classical geodesics and does not compute absorption amplitudes or conditional radiation states.

The quantum model further assumes local orthogonal effective states, a subsystem factorization and a chosen postselected ensemble. These are not consequences of the first law. A fully specified calculation would need incoming finite wavepackets with their polarization and angular-momentum distributions; mode-dependent absorption and any outgoing modes; black-hole and environmental initial states; the definition of dressed, relational or asymptotic observables; and the source, reference-frame and conservation bookkeeping. It would then need to determine whether a phase-sensitive observable can be accessed outside the horizons without relying on an operation prohibited by the relevant classical or quantum constraints. Until such a construction is supplied, the coherence witness remains a well-defined algebraic target rather than an experimental proposal.

The linked comparison therefore identifies a definite modelling target: calculate the capture instrument and its radiative records, then determine which exterior observables retain sensitivity to the conditional phase. The classical area response supplies the reference against which that calculation can be assessed.

7 Conclusion

In an ideal local recoil model, momentum exchange correlates each photon path with a mass state. The overlap of the joint mass records determines the remaining two-photon coherence and

concurrence; ordinary outcome correlations can remain when the photons alone have become an incoherent mixture. The full photon–mass entanglement across the two sides is preserved by the assumed local unitaries.

For two symmetric Kerr encounters, the first law gives unequal positive area increases for the chosen aligned and opposed deposits. Reversing both incoming sides exchanges which hole receives the larger increase, with the same leading total. This statement is a classical, model-dependent benchmark. An effective two-hole state can retain coherence between the two allocations, but this requires additional assumptions about the states, subsystem split and external records. A phase-sensitive witness distinguishes the conditional coherent model from the specified diagonal mixture, while its physical implementation remains unresolved.

The capture map isolates the dynamical information needed for a more complete treatment: mode-resolved amplitudes, the overlap of the associated field records and a specification of accessible observables and reference systems. Calculating these quantities would connect the phase-sensitive benchmark to a concrete quantum scattering model.

A Kerr capture and first-law checks

For the geodesic check, temporarily use geometrized units $G = c = M = 1$. Write the radial Boyer–Lindquist coordinate as $x = r/r_g$, the spin parameter as $a = a_*$ and the signed impact parameter as $\xi = b/r_g$. For equatorial massless motion the radial potential can be written $\mathcal{R}/x = f_\xi(x)$, with [13]

$$f_\xi(x) = x^3 + (a^2 - \xi^2)x + 2(\xi - a)^2. \tag{29}$$

For $a = 1/2$ and $\xi = +1$ or -1,

$$f_{+1}(x) = x^3 - \tfrac{3}{4}x + \tfrac{1}{2}, \qquad f_{-1}(x) = x^3 - \tfrac{3}{4}x + \tfrac{9}{2}. \tag{30}$$

The outer horizon is at $x_+ = 1+\sqrt{3}/2$. Both polynomials are positive there, and $f'_\xi(x) = 3x^2 - 3/4 > 0$ for all $x \geq x_+$. They therefore have no zero outside the horizon for these parameters. The ingoing solution can cross it in the classical test-ray model. The signs in Eq. (2) are determined separately by the global geometry; the $\xi = \pm 1$ calculation checks both possibilities.

The first-law result can be checked directly by differentiating the exact Kerr area. In SI units define the dimensionless mass ratio $m = M'/M$ and dimensionless angular-momentum variable $j = cJ'/(GM^2)$, relative to the *initial* M. Then

$$A(M', J') = 8\pi r_g^2 \left(m^2 + \sqrt{m^4 - j^2} \right). \tag{31}$$

At $m = 1$, $j = a_*$, an ideal deposited energy E and $L = Er_g/c$ give $m = 1 + \epsilon$, $j = a_* \pm \epsilon$, where $\epsilon = E/(Mc^2)$. Differentiation yields

$$\frac{1}{8\pi r_g^2} \frac{\mathrm{d}A}{\mathrm{d}\epsilon}\bigg|_{\pm} = 2 + \frac{2 \mp a_*}{\sqrt{1 - a_*^2}}. \tag{32}$$

These slopes agree with Eqs. (10)–(12). In the numerical example ϵ is so small that ordinary double-precision subtraction of the two large areas would lose the difference; the accompanying check uses high-precision decimal arithmetic. The first-order approximation does not supply an independent uncertainty estimate for unmodelled physics.

B Reproduction of the numerical and witness results

The accompanying calculation files evaluate Eqs. (3), (8), (9)–(12), the cubic capture check, the conditional capture state, the response covariance and the algebraic witness bound. Inputs are $G = 6.67430 \times 10^{-11}\,\mathrm{m^3\,kg^{-1}\,s^{-2}}$, $c = 299792458\,\mathrm{m\,s^{-1}}$, $h = 6.62607015 \times 10^{-34}\,\mathrm{J\,s}$, $1\,\mathrm{eV} = 1.602176634 \times 10^{-19}\,\mathrm{J}$, and $\hbar = h/(2\pi)$, using the recommended constants compilation [10]. The chosen object parameters are stated in Secs. 3 and 4.2; no fitted values or observations enter.

For the witness, the computational basis ordering is $00, 01, 10, 11$. Equation (26) couples only 01 and 10. Its separability bound follows analytically from the local Bloch-vector argument in Sec. 5.1; numerical matrix calculations are a check, not a proof based on a finite sample. For the exact two-alternative state in Eq. (21), the partial transpose has eigenvalues p, $1 - p$, $|z|$ and $-|z|$, establishing nonseparability for $z \neq 0$ in this two-qubit model.

Acknowledgments

The author acknowledges CERN colleagues for useful discussions.

Declarations

The author declares no conflicts of interest. Also that no funding was used for the elaboration of the manuscript. No new data was generated.

References

[1] William Donnelly and Steven B. Giddings. Gravitational splitting at first order: Quantum information localization in gravity. *Physical Review D*, 98:086006, 2018. doi: https://doi.org/10.1103/PhysRevD.98.086006.

[2] Daine L. Danielson, Gautam Satishchandran, and Robert M. Wald. Black holes decohere quantum superpositions. *International Journal of Modern Physics D*, 31(14):2241003, 2022. doi: https://doi.org/10.1142/S0218271822410036.

[3] Joshua Foo, Robert B. Mann, and Magdalena Zych. Schrödinger's black hole cat. *International Journal of Modern Physics D*, 31:2242016, 2022. doi: https://doi.org/10.1142/S0218271822420160.

[4] Joshua Foo, Robert B. Mann, and Magdalena Zych. Signatures of discretization in quantum black hole spectra. *International Journal of Modern Physics D*, 32(14):2342015, 2023. doi: https://doi.org/10.1142/S0218271823420154.

[5] Yuxuan Liu, Zhuo-Yu Xian, Cheng Peng, and Yi Ling. Black holes entangled by radiation. *Journal of High Energy Physics*, 2022(9):179, 2022. doi: https://doi.org/10.1007/JHEP09(2022)179; erratum: https://doi.org/10.1007/JHEP11(2022)024; addendum: https://doi.org/10.1007/JHEP11(2022)043.

[6] Kamil Brádler and Christoph Adami. The capacity of black holes to transmit quantum information. *Journal of High Energy Physics*, 2014(5):095, 2014. doi: https://doi.org/10.1007/JHEP05(2014)095.

[7] Samuel E. Gralla and Hongji Wei. Decoherence from horizons: General formulation and rotating black holes. *Physical Review D*, 109(6):065031, 2024. doi: https://doi.org/10.1103/PhysRevD.109.065031.

[8] Luiz C. S. Leite, Sam R. Dolan, and Luís C. B. Crispino. Absorption of electromagnetic and gravitational waves by Kerr black holes. *Physics Letters B*, 774:130–134, 2017. doi: https://doi.org/10.1016/j.physletb.2017.09.048.

[9] Berthold-Georg Englert. Fringe visibility and which-way information: An inequality. *Physical Review Letters*, 77:2154–2157, 1996. doi: https://doi.org/10.1103/PhysRevLett.77.2154.

[10] National Institute of Standards and Technology. CODATA recommended values of the fundamental physical constants: 2022, 2024. NIST SP 961, https://physics.nist.gov/cuu/pdf/wall_2022.pdf.

[11] O. Ruiz, U. Molina, and P. Viloria. Thermodynamic analysis of Kerr-Newman black holes. *Journal of Physics: Conference Series*, 1219:012016, 2019. doi: https://doi.org/10.1088/1742-6596/1219/1/012016.

[12] J. M. Bardeen, B. Carter, and S. W. Hawking. The four laws of black hole mechanics. *Communications in Mathematical Physics*, 31:161–170, 1973. doi: https://doi.org/10.1007/BF01645742.

[13] Lev Morgovsky. Critical equatorial trajectories of massless particles in a Kerr spacetime. *Journal of High Energy Physics, Gravitation and Cosmology*, 8:647–656, 2022. doi: https://doi.org/10.4236/jhepgc.2022.83047.

[14] Maulik Parikh and Jude Pereira. Quantum uncertainty in the area of a black hole. *Journal of High Energy Physics*, 2025(9):137, 2025. doi: https://doi.org/10.1007/JHEP09(2025)137.

[15] Stephen W. Hawking. Gravitational radiation from colliding black holes. *Physical Review Letters*, 26:1344–1346, 1971. doi: https://doi.org/10.1103/PhysRevLett.26.1344.

[16] D. Kafri, J. M. Taylor, and G. J. Milburn. A classical channel model for gravitational decoherence. *New Journal of Physics*, 16:065020, 2014. doi: https://doi.org/10.1088/1367-2630/16/6/065020.

[17] Juan Maldacena and Leonard Susskind. Cool horizons for entangled black holes. *Fortschritte der Physik*, 61(9):781–811, 2013. doi: https://doi.org/10.1002/prop.201300020.

[18] Vijay Balasubramanian, Micha Berkooz, Simon F. Ross, and Joan Simón. Black holes, entanglement and random matrices. *Classical and Quantum Gravity*, 31(18):185009, 2014. doi: https://doi.org/10.1088/0264-9381/31/18/185009.

[19] Samuel L. Braunstein and Arun K. Pati. Quantum information cannot be completely hidden in correlations: Implications for the black-hole information paradox. *Physical Review Letters*, 98:080502, 2007. doi: https://doi.org/10.1103/PhysRevLett.98.080502.

[20] Shahar Hod. Bohr's correspondence principle and the area spectrum of quantum black holes. *Physical Review Letters*, 81:4293, 1998. doi: https://doi.org/10.1103/PhysRevLett.81.4293.

[21] Michele Maggiore. Physical interpretation of the spectrum of black hole quasinormal modes. *Physical Review Letters*, 100:141301, 2008. doi: https://doi.org/10.1103/PhysRevLett.100.141301.

[22] Gilad Gour and A. J. M. Medved. The Kerr black hole as a quantum rotator. *Classical and Quantum Gravity*, 20(11):2261, 2003. doi: https://doi.org/10.1088/0264-9381/20/11/321.